The Astrophysical Journal, 925:169 (8pp), 2022 February 1 https://doi.org/10.3847/1538-4357/ac409b

Revisiting the Lensed Fraction of High-redshift Quasars

Minghao Yue, Xiaohui Fan, Jinyi Yang[1], and Feige Wang[2]
Steward Observatory, University of Arizona, 933 North Cherry Avenue, Tucson, AZ 85721, USA; yuemh@email.arizona.edu
Received 2021 October 13; revised 2021 December 2; accepted 2021 December 5; published 2022 February 3

Abstract

The observed lensed fraction of high-redshift quasars (∼0.2%) is significantly lower than previous theoretical predictions (≳4%). We revisit the lensed fraction of high-redshift quasars predicted by theoretical models, where we adopt recent measurements of galaxy velocity dispersion functions (VDFs) and explore a wide range of quasar luminosity function (QLF) parameters. We use both analytical methods and mock catalogs, which give consistent results. For ordinary QLF parameters and the depth of current high-redshift quasar surveys ($m_z \lesssim 22$), our model suggests a multiply imaged fraction of $F_{\rm multi} \sim 0.4\%$–0.8%. The predicted lensed fraction is ∼1%–6% for the brightest $z_s \sim 6$ quasars ($m_z \lesssim 19$), depending on the QLF. The systematic uncertainties of the predicted lensed fraction in previous models can be as large as 2–4 times and are dominated by the VDF. Applying VDFs from recent measurements decreases the predicted lensed fraction and relieves the tension between observations and theoretical models. Given the depth of current imaging surveys, there are ∼15 lensed quasars at $z_s > 5.5$ detectable over the sky. Upcoming sky surveys like the Legacy Survey of Space and Time survey and the Euclid survey will find several tens of lensed quasars at this redshift range.

Unified Astronomy Thesaurus concepts: Quasars (1319); Strong gravitational lensing (1643)

1. Introduction

In the past two decades, extensive searches have been carried out for high-redshift quasars (e.g., Jiang et al. 2016; Matsuoka et al. 2018; Wang et al. 2019, 2021; Yang et al. 2019b, 2020), which led to a sample of more than 1200 quasars at $z > 4.5$ (more than 500 at $z > 5$). In Fan et al. (2019), we reported the discovery of the first gravitationally lensed quasar at $z > 5$ (J0439+1634 at $z = 6.52$). High-redshift lensed quasars such as J0439+1634 are valuable, as they enable in-depth investigations of distant quasars with enhanced sensitivity and resolution (e.g., Yang et al. 2019a; Yue et al. 2021).

Since the commissioning of the Sloan Digital Sky Survey (SDSS; York et al. 2000), there have been efforts to search for lensed quasars at $z \gtrsim 4$ (e.g., Richards et al. 2004, 2006). However, there are only three lensed quasars at $z > 4.5$ known so far, including a couple at $z = 4.8$ (McGreer et al. 2010; More et al. 2016) and J0439+1634 at $z = 6.52$. The fraction of lensed ones among high-redshift quasars is ∼0.2% (without correcting for survey incompleteness). Meanwhile, a number of theoretical studies have predicted a high lensed fraction (≳4%) for high-redshift quasars due to strong magnification bias (e.g., Comerford et al. 2002; Wyithe & Loeb 2002; Pacucci & Loeb 2019). Fan et al. (2019) and Pacucci & Loeb (2019) suggested that survey incompleteness is a plausible reason for the discrepancy.

We notice, however, that previous models were based on various assumptions on the quasar population and the deflector population, which might introduce systematic errors that have not been fully explored. In particular, many previous studies were based on early measurements of quasar luminosity functions (QLFs) and deflector velocity dispersion functions (VDFs). Since recent observations have provided more accurate measurements of the QLFs and VDFs, there is a need to re-investigate the models of high-redshift lensed quasars in order to fully understand the discrepancy between theoretical predictions and observations.

In this paper, we revisit the models of high-redshift lensed quasar population and investigate possible systematic uncertainties. We adopt recent measurements of VDFs and QLFs, and use both analytical methods and mock catalogs to model the properties of high-redshift lensed quasars. Our analysis addresses the following questions: (1) what are the uncertainties of the theoretical models, (2) how many lensed quasars can we detect in current and future sky surveys, and (3) how strong is the tension between the theoretical predictions and the observations? Answering these questions is critical to the design of a complete search for high-redshift lensed quasars with upcoming sky surveys like the Vera C. Rubin Observatory Legacy Survey of Space and Time (LSST; Ivezić et al. 2019).

This paper is organized as follows. We describe the analytical method in Section 2, and the mock catalog method in Section 3. We present the predicted statistics of high-redshift lensed quasars in Section 4, discuss the implications in Section 5, and summarize our conclusions in Section 6. We use a flat ΛCDM cosmology with $H_0 = 70\,{\rm km\,s^{-1}\,Mpc^{-1}}$ and $\Omega_M = 0.3$ throughout this work. All magnitudes are z-band AB magnitudes unless further specified.

2. Analytical Method

In this section, we describe the analytical model of the high-redshift lensed quasar population, including the lensing model, the deflector galaxies, and the source quasars. In this paper, we use "strongly lensed" and "multiply imaged" interchangeably.

2.1. Lensing Models

We use singular isothermal spheres (SIS) to describe the mass profile of deflector galaxies. SIS and singular isothermal

[1] Strittmatter Fellow.
[2] NHFP Hubble Fellow.

ellipsoids (SIE; e.g., Kormann et al. 1994) are widely used in models of strong-lensing systems (e.g., Wyithe & Loeb 2002; Oguri & Marshall 2010). SIS is parameterized by its Einstein radius, $\theta_{\rm E} = 4\pi\left(\frac{\sigma}{c}\right)^2\frac{D_{ds}}{D_s}$, where σ is the velocity dispersion of the deflector, and D_{ds} and D_s are the angular diameter distances from the source to the deflector and the observer, respectively. Following Wyithe et al. (2011), the lensing optical depth of a population of SIS deflectors, i.e., the probability for a source at redshift z_s to be multiply imaged, is

$$\tau_m = \int_0^{z_s} dz_d \int d\sigma \phi(\sigma, z_d)\frac{d^2V_c}{d\Omega dz_d}\pi\theta_{\rm E}(\sigma, z_d, z_s)^2 D_d^2, \quad (1)$$

where z_d is the deflector redshift, $\phi(\sigma, z_d)$ is the deflector VDF, $\frac{d^2V_c}{d\Omega dz_d} = (1+z_d)^3 c\frac{dt}{dz_d}$ is the differential comoving volume, and D_d is the angular diameter distance at z_d.

The lensing optical depth τ_m describes the fraction of lensed ones among *all* background sources. In flux-limited surveys, however, some lensed sources that are intrinsically fainter than the survey limit can still be detected. Consequently, we expect that the observed lensed fraction in flux-limited surveys should be higher than τ_m. The magnification bias B quantifies this effect,

$$B = \frac{\int_{\mu_{\rm min}}^{+\infty} d\mu\, p(\mu) N(>L_{\rm lim}/\mu)}{N(>L_{\rm lim})}, \quad (2)$$

where $p(\mu)$ is the probabilistic distribution of the magnification of lensed sources, $L_{\rm lim}$ is the survey flux limit, and $N(>L_{\rm lim})$ is the number of background sources brighter than $L_{\rm lim}$. According to Equation (2), if there are $N(>L_{\rm lim})$ strongly lensed objects that are intrinsically brighter than $L_{\rm lim}$, the number of strongly lensed objects that have magnified flux brighter than $L_{\rm lim}$ should be $B \times N(>L_{\rm lim})$.

In our analytical model, we use $\mu_{\rm min} = 2$, which is the minimum magnification for multiply imaged systems generated by SIS. If the survey has a high spatial resolution that can resolve the lensing structure, we shall use $p(\mu) = 2/(\mu-1)^3$, which describes the magnification of the brighter lensed image. Similarly, for surveys with poor resolution where the lensed images are blended, we use $p(\mu) = 8/\mu^3$, which corresponds to the total magnification.[3] Although SIS deflectors cannot produce quad lenses, the fraction of quad lenses among all lenses is small (∼10%, e.g., Oguri & Marshall 2010).

The fraction of lensed sources among all sources that have *apparent* luminosity brighter than $L_{\rm lim}$ is (e.g., Mason et al. 2015):

$$F_{\rm multi} = \frac{B\tau_m}{B\tau_m + B'(1-\tau_m)}, \quad (3)$$

where B' is the magnification bias of sources that are not multiply imaged. The major source of B' is weak lensing. As shown in Mason et al. (2015), for sources at $z_s > 6$, the magnifications caused by weak lensing ($\mu_{\rm weak}$) are distributed within a narrow range around $\mu_{\rm weak} \approx 1$, with almost all sources have $0.7 < \mu_{\rm weak} < 1.3$. According to Equation (2), we use $B' \approx 1$ in our model. This approximation is also adopted in Wyithe et al. (2011).

[3] We derive $p(\mu)$ from Equations 8.34(c)–8.35(b) from Schneider et al. (1992). Also see Wyithe et al. (2011).

2.2. Deflector Population

The observed galaxy VDFs are well-described by Schechter functions (e.g., Choi et al. 2007; Chae 2010). In this work, we use the following form of the Schechter function:

$$\phi(\sigma, z_d)d\sigma = \phi_*\left(\frac{\sigma}{\sigma_*}\right)^a \exp\left[-\left(\frac{\sigma}{\sigma_*}\right)^b\right]\frac{d\sigma}{\sigma}, \quad (4)$$

where $\phi(\sigma, z_d)d\sigma$ is the number density of galaxies at redshift z_d that have velocity dispersions within $(\sigma, \sigma + d\sigma)$. In principle, the parameters ϕ_*, σ_*, a, and b may evolve with redshift. We adopt the parameterized local VDF from Hasan & Crocker (2019) and assume the redshift evolution of ϕ_* and σ_* suggested by Geng et al. (2021). The resulting VDF has $\phi_* = 6.92 \times 10^{-3}(1+z_d)^{-1.18}\,{\rm Mpc}^{-3}$, $\sigma_* = 172.2 \times (1+z_d)^{0.18}$ km s^{-1}, $a = -0.15$ and $b = 2.35$. In Figure 1, we compare our parameterized VDF and the observed values in the local universe from Sohn et al. (2017) and Hasan & Crocker (2019), and at $0.3 < z_d < 1.5$ from Bezanson et al. (2012). This parameterized, redshift-evolving VDF is in good agreement with the observations at $z_d < 1.5$, which cover the majority of the deflector population (Section 4.1).

2.3. Quasar Luminosity Functions

QLFs are usually parameterized by a broken power law (Pei 1995), which accurately describes the QLF at all redshifts (e.g., Kulkarni et al. 2019):

$$\Phi(M, z_s) = \frac{\Phi^*(z_s)}{10^{0.4(\alpha+1)(M-M^*)} + 10^{0.4(\beta+1)(M-M^*)}}, \quad (5)$$

where α and β are the faint- and bright-end slopes, M^* is the break magnitude, and Φ^* is the normalization. For M and M^*, we use the absolute magnitude at rest-frame 1450 Å (M_{1450}) throughout this paper. We use the median value of $m - M_{1450}$ of $z_s \sim 6$ mock quasars (Section 3) to convert apparent magnitudes m to absolute magnitudes. Since the shape of QLF determines the magnification bias, we explore a wide range of α, β, and M^* values in Section 4.2. The normalization Φ^* has no impact on the magnification bias and thus the multiply imaged fraction.

3. Mock Catalog Method

In addition to the analytical model, we also use mock catalogs to investigate the lensed quasar population. The mock catalogs not only serve as independent tests that validate the analytical model, but also illustrate the impact of some simplifications, e.g., using SIS instead of SIE to describe deflectors. The methods of mock catalog generation are described in M. Yue et al. (2021, in preparation) and briefly summarized here.

We use the CosmoDC2 mock galaxy catalog (Korytov et al. 2019) to model the deflector galaxy population. CosmoDC2 is a synthetic mock catalog that covers a sky area of 440 deg^2 and out to redshift $z = 3$. We use SIEs to describe the mass profile of the deflector galaxies. CosmoDC2 provides the mass, half-light radius, and ellipticity of each mock galaxy, and we estimate the velocity dispersion using a simple relation based on the virial theorem. The resulting VDF is shown in Figure 1,

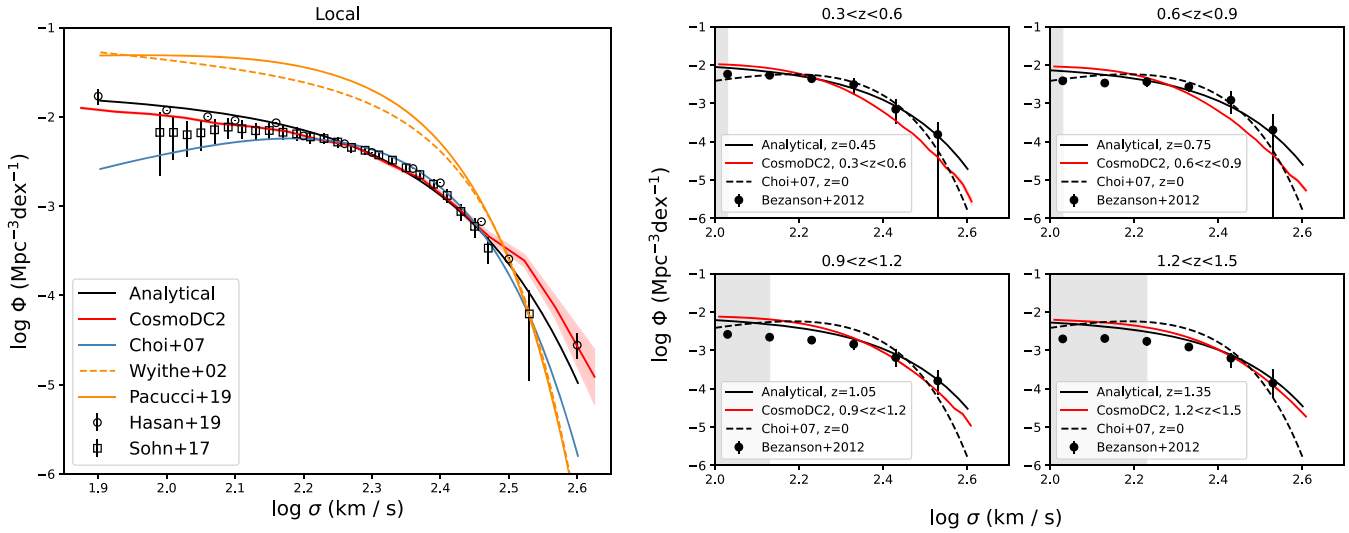

Figure 1. The velocity dispersion functions. Left: the local VDF. The black solid line shows the analytical VDF adopted by this work, and the red solid line illustrates the VDF of the CosmoDC2 catalog. The open squares and circles are the observed VDFs from Sohn et al. (2017) and Hasan & Crocker (2019). All these VDFs are in good agreement with each other. We also include the VDFs used in previous studies of high-redshift lensed quasars for comparison (Section 5). Right: the VDF beyond the local universe. The black dots are the observed VDF from Bezanson et al. (2012), and the gray area marks the mass range where Bezanson et al. (2012) suggested that their galaxy sample has low completeness. Both the analytical VDF and the CosmoDC2 VDF are consistent with the observed ones except at the low-mass end, which could be a result of the incompleteness of the observed galaxy sample. We also include the local VDF from Choi et al. (2007) (black dashed line), which has been used in previous studies to model the deflectors.

which is consistent with observations and is in good agreement with the analytical VDF out to $z_d \sim 1.5$.

We then generate two types of mock background sources to study the statistics related to τ_m and B, respectively:

1. Sources at fixed redshifts. They are used to model the redshift evolution of τ_m. Since the CosmoDC2 catalog only contains mock galaxies at $z_d < 3$, it does not provide complete descriptions of the deflectors for sources at $z_s > 3$. As such, we generate three sets of mock sources at $z_s = 1$, 2, and 3.
2. Simulated quasars at $5.5 < z_s < 6.5$, which are used to investigate the impact of QLF parameters on the magnification bias, B, for quasars at $z_s \sim 6$. We generate these simulated quasars using SIMQSO (McGreer et al. 2013). SIMQSO generates mock quasar catalogs with simulated spectra according to the input QLF. Specifically, we consider two sets of QLFs: the "steep" set, which has $\alpha = -2$, $M^* = -27$ (e.g., McGreer et al. 2018), and the "shallow" set, which has $\alpha = -1.3$, $M^* = -25$ (e.g., Matsuoka et al. 2018). For each set, we consider a range of bright-end slopes at $-3.4 \leqslant \beta \leqslant -2.6$. We adopt the normalization Φ^* from Matsuoka et al. (2018).

We assign random positions to the sources in the CosmoDC2 field, and use `GLAFIC` (Oguri 2010) to perform lens modeling and identify multiply imaged systems. For the second type of sources (i.e., mock quasars), we run multiple random realizations to suppress the Poisson noise, such that the number of lensed quasars are equivalent to 20× sky area.

It is useful to keep in mind the differences between the mock catalog and the analytical model. The VDFs of the two approaches are close but have small differences, and we use SIE instead of SIS to model the deflectors for mock catalogs. Besides, the mock quasars generated by SIMQSO have a variety of continuum slopes and emission line properties to match the observed distribution, while in the analytical model, we perform a simple k-correction to convert absolute to apparent magnitudes. As a result, we do not expect that the two methods should give the same result. Nonetheless, as we will show in Section 4, the predictions of the two approaches are largely consistent, which suggests that both approaches are solid.

4. Results

We focus on the multiply imaged fraction $F_{\rm multi}$ of $z_s \sim 6$ quasars in this work. According to Equation (3), $F_{\rm multi}$ is a function of the lensing optical depth τ_m and the magnification bias B. We describe the two factors respectively in the following subsections.

4.1. Lensing Optical Depth

We first present the lensing optical depth, τ_m, predicted by the analytical model and the mock catalog. Since the CosmoDC2 catalog does not have galaxies at $z_d > 3$, we only use the mock catalog to calculate the lensing optical depth for sources at $z_s \leqslant 3$. In general, we validate our methods by comparing the mock catalog and the analytical model at $z_s \leqslant 3$, and make predictions using the analytical model at higher redshifts.

The left panel of Figure 2 illustrates the predicted lensing optical depth as a function of source redshift z_s. At $z_s \leqslant 3$, the outputs of the analytical model and the mock catalog are similar. This comparison suggests that both the analytical method and the mock catalog method are reliable. We use the analytical model to predict the lensing optical depth at $z_s > 3$, which gives $\tau_m = 1.8 \times 10^{-3}$ for $z_s = 6$.

To further validate our analysis, we include two additional experiments: the "CosmoDC2 Discrete Sum" where we change the integration in Equation (1) to discrete sums and calculate τ_m using the CosmoDC2 VDF; and the "Mock Catalog SIS," where we use SIS instead of SIE deflectors when making the mock catalogs. In other words, the two experiments calculate

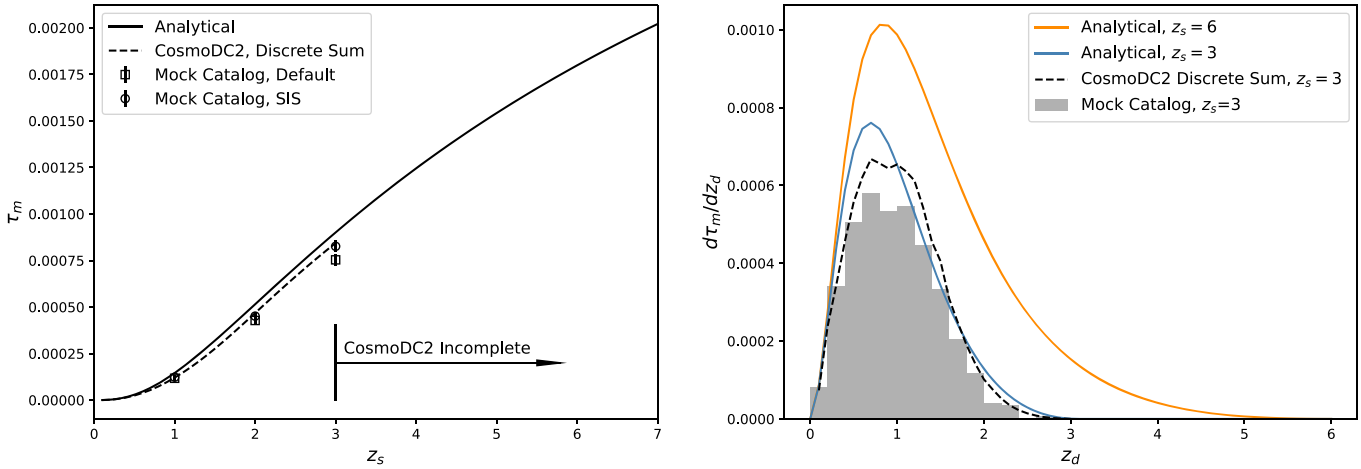

Figure 2. Left: the lensing optical depth as a function of source redshift. Note that the CosmoDC2 catalog do not contain deflectors at $z_d > 3$, so the mock catalog is incomplete at $z_s > 3$. The analytical model has $\tau_m = 1.8 \times 10^{-3}$ at $z_s = 6$. At $z_s < 3$, the outputs of the analytical model and the mock catalog are similar. We include two additional experiments to validate the results, the CosmoDC2 Discrete Sum and the Mock Catalog SIS, which further demonstrate that our analysis is reliable (see text for details). Right: the distribution of deflector redshifts. For $z_s = 6$, the analytical model suggests that most of the deflectors have $0.5 < z_d < 2.5$, and the distribution peaks at $z_d \sim 1$. We also include the predictions for $z_s = 3$ as a test of our results, for which the analytical method is consistent with the mock catalog.

τ_m using the analytical method and the mock catalog method assuming the same VDF and deflector mass profile. Figure 2 shows that the two experiments provide the same result, further proving that both methods are reliable. The comparison between the default mock catalogs and the Mock Catalog SIS suggests that using SIS instead of SIE will overestimate the lensing optical depth by ∼10%. This is consistent with the result in Kormann et al. (1994), who show that the cross section of an SIE decreases with ellipticity.

In the right panel of Figure 2, we show the redshift distribution of the deflector galaxies for sources at $z_s = 6$, predicted by the analytical model. We also include the predictions for $z_s = 3$ from both the analytical model and the mock catalog for comparison. Again, the two methods give very similar results for $z_s = 3$. For sources at $z_s = 6$, the distribution of deflectors peaks at $z_d \sim 1$, and the majority of deflector galaxies have $0.5 \lesssim z_d \lesssim 2.5$. It is thus important to correctly model the redshift evolution of VDF out to $z_d \gtrsim 2$ in order to make precise predictions of τ_m for high-redshift sources.

It is worth noticing that the analytical model gives a higher lensing optical depth than the mock catalogs. The reason is that the analytical VDF is higher than the CosmoDC2 VDF at $z_d \sim 0.6$ (as shown in Figure 1) and $z_d \gtrsim 2$. Since VDFs beyond the local universe have yet to be well-constrained by observations, the predicted lensing optical depth will inevitably have some systematic errors. We will discuss this point in more detail in Section 5.1.

Figure 3 shows the distribution of lensing separation for $z_s = 6$ sources. About 65% (85%) of the lenses have separation larger than 1″ (0.″5). Most of these lenses will be resolved in surveys such as the LSST, which has a seeing of ∼0.″7. The only lensed quasar at $z > 5$ known to date, J0439+1634 at $z = 6.52$, is a compact system with $\Delta\theta = 0.''2$. Figure 3 suggests that such systems are rare but possible.

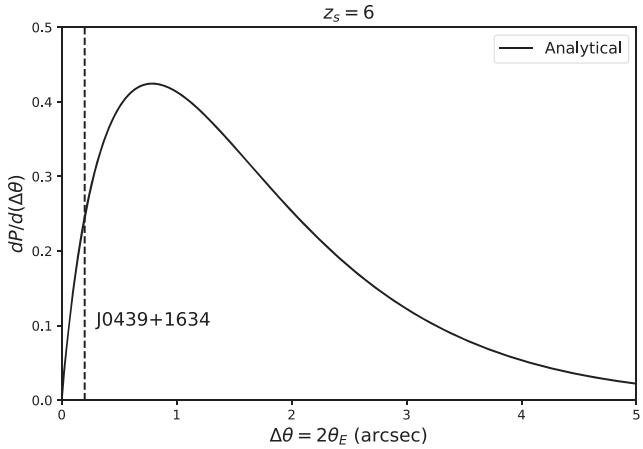

Figure 3. Distribution of the lensing separation for sources at $z_s = 6$, predicted by the analytical model. About 85% of the lenses have $\Delta\theta > 0.''5$, and the fraction is ∼65% for $\Delta\theta > 1.''0$. The dashed line shows the separation of J0439+1634 at $z_s = 6.52$, which is the only known lensed quasar at $z_s > 5$. Systems like J0439+1634 are rare but are still possible.

4.2. Magnification Bias and the Lensed Fraction

The magnification bias B is a function of the QLF and $p(\mu)$ (Equation (2)). We use both the analytical model and the mock catalogs to calculate the magnification bias. Note that, although the mock catalogs do not have deflectors at $z_d > 3$, they still provide correct descriptions for the magnification biases of high-redshift sources, since z_d and the VDF do not go into the calculation of B.

Figure 4 shows the predicted magnification bias as a function of QLF parameters. We consider two specific cases, where the top panel shows the magnification bias for the brightest lensed image (B_1) and the lower panel shows the bias for the total magnification ($B_{\rm total}$). According to Figure 4, the magnification biases of the two cases differ by ∼50%. Observationally, these two cases correspond to the high and low spatial resolution limits, respectively, and real surveys lie between the two special cases.

The predictions of the analytical model and the mock catalogs are consistent in all cases. This comparison suggests that using SIS in the analytical model gives a good approximation of the real case where deflectors are elliptical. The magnification bias is higher for steeper bright-end slope and decreases with the survey depth, which is a result of the flatter faint-end slope compared to the bright-end. To calculate

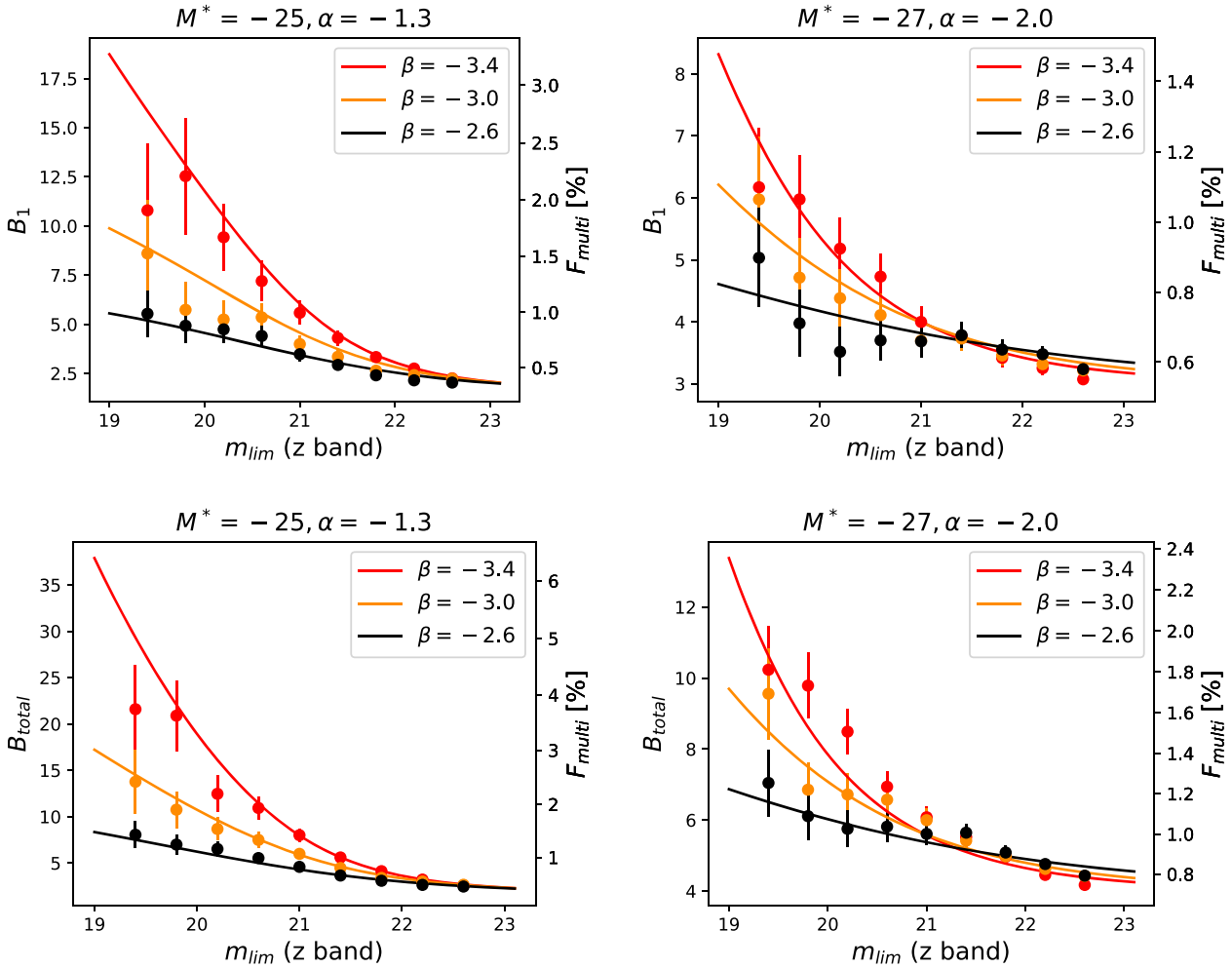

Figure 4. The magnification bias of $z_s \sim 6$ lensed quasars as a function of QLF parameters. We illustrate two cases, where the top panel shows the magnification bias for the brightest lensed image, and the bottom panel is for the total flux of all lensed images. In all cases, the analytical model (solid lines) agrees well with the mock catalog (dots with error bars), suggesting that the difference between SIS and SIE deflectors is small. We assume Poisson statistics for the mock catalog (note that the mock catalogs are equivalent to 20× sky area). The secondary y-axis marks the multiply imaged fraction assuming $\tau_m = 1.8 \times 10^{-3}$. The magnification bias is higher for steeper faint-end slope and drops with survey depth. For the depth of current surveys of high-redshift quasars ($m_{\rm lim} \sim 22$), the lensed fraction is $F_{\rm multi} \sim 0.4\%$–0.8%.

the lensed fraction $F_{\rm multi}$, we adopt $\tau_m = 1.8 \times 10^{-3}$ for $z_s = 6$. High-redshift quasar searches in the SDSS have a depth of $m_{\rm lim} = 20.2$ (e.g., Richards et al. 2002), for which the lensed fractions is $F_{\rm multi} \sim 1\%$–3%. Present-day surveys for $z \sim 6$ quasars usually have $m_{\rm lim} \gtrsim 22$ (e.g., Jiang et al. 2016; Matsuoka et al. 2018), which corresponds to $F_{\rm multi} \sim 0.4\%$–0.8%. The lensed fraction of the brightest $z_s \sim 6$ quasar population ($m_z \lesssim 19$) can be as high as $\sim$6% for the steep bright-end slopes.

In Figure 5, we further explore the impact of QLF parameters on the lensed fraction using the analytical model. Note that an absolute magnitude of -25 corresponds to an apparent magnitude of 21.5 at $z_s = 6$ under our assumed k-correction. The multiply imaged fraction can be as high as $\gtrsim$10% at the corner of $M_{\rm lim} - M^* \lesssim -2$ and $\beta \lesssim -3.5$. The lensed fraction drops quickly to other regions. In particular, we highlight the predictions for our fiducial QLF of $\alpha = -1.3$, $\beta = -2.75$, and $M^* = -25$, which are close to the measurements in Matsuoka et al. (2018) and Wang et al. (2019) for $z_s \gtrsim 6$ quasars. This fiducial QLF gives $F_{\rm multi} \sim 1\%$–2% for the brightest quasars ($m_z \lesssim 19$) and $F_{\rm multi} \sim 0.4\%$–0.8% for a survey depth of $m_z \approx 22$.

5. Discussion

5.1. The Lensed Fraction of High-redshift Quasars

We can now investigate the discrepancy between observations and theoretical models in the lensed fraction of high-redshift quasars. According to Equation (3), the multiply imaged fraction $F_{\rm multi}$ is a function of the lensing optical depth τ_m and the magnification bias B. We first consider the lensing optical depth τ_m, which is determined by the deflector VDF. Figure 1 summarizes the VDFs adopted by previous models of high-redshift lensed quasars. In general, two approaches have been adopted to model the deflector VDF:

(1) Convert galaxy luminosity functions to VDFs using empirical relations such as the Faber–Jackson relation (FJR; Faber & Jackson 1976). This method was used in Wyithe & Loeb (2002) and Pacucci & Loeb (2019). Figure 1 shows that the VDFs in these two studies are close to each other, and both of them are significantly higher than the observed VDFs. Correspondingly, both studies predicted a lensed fraction that is several times higher than our model ($F_{\rm multi} \gtrsim 5\%$ for $m_{\rm lim} = 20.2$). The reason why FJR leads to a high VDF is complicated. First, the FJR has a large scatter ($\gtrsim$10 km s^{-1},

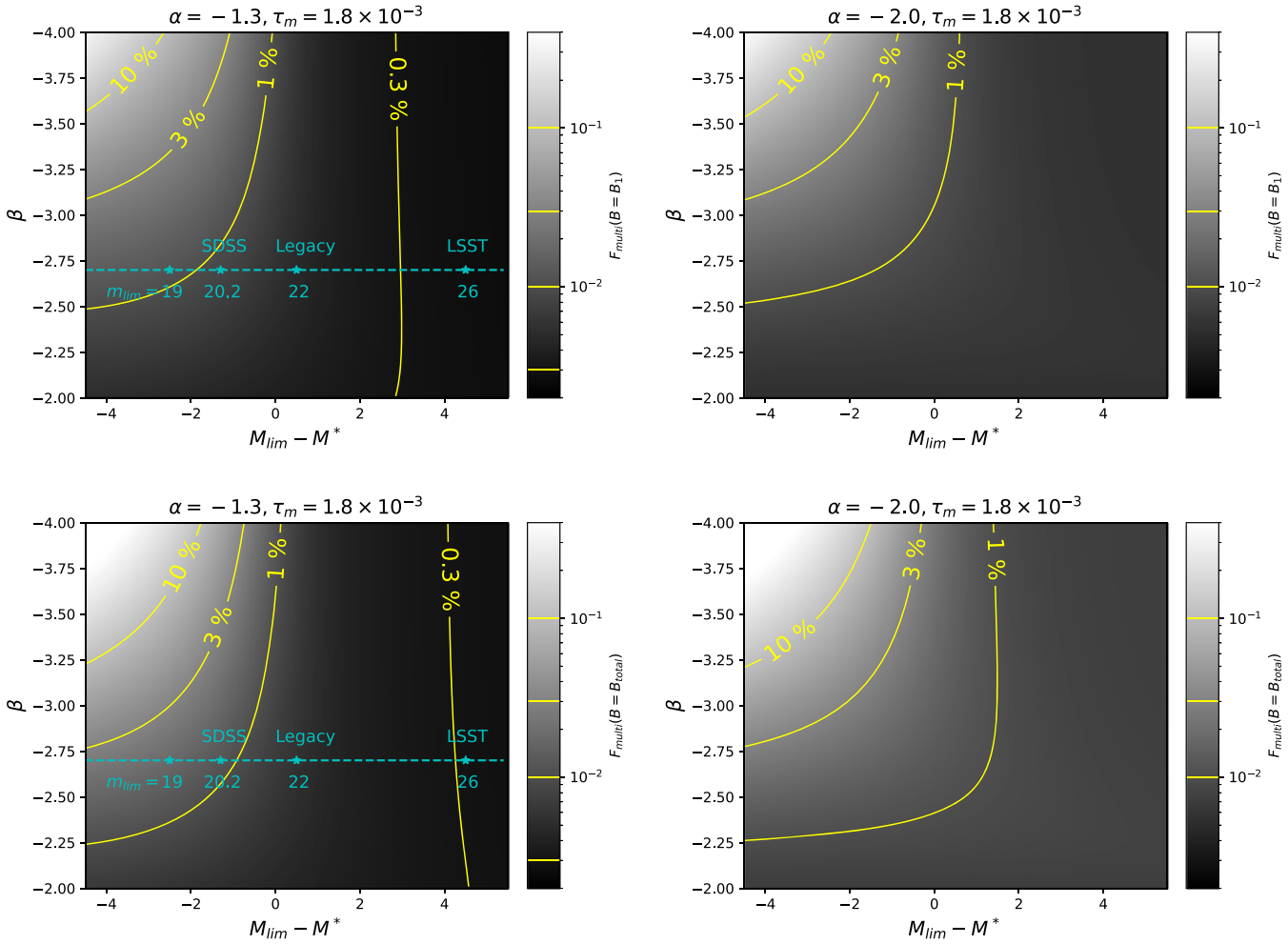

Figure 5. Lensed fraction of $z_s \sim 6$ quasars as a function of QLF parameters, predicted by the analytical model. Similar to Figure 4, we assume $\tau_m = 1.8 \times 10^{-3}$, and illustrate the two cases that correspond to the brightest image (top) and the total flux (bottom). The contours mark levels of 10%, 3%, 1%, and 0.3%, and these levels are also marked in the color bars by yellow lines. For shallow surveys ($M_{\rm lim} - M^* \lesssim -2$) and steep bright-end slopes ($\beta \lesssim -3.5$), the lensed fraction can be as high as $F_{\rm multi} \gtrsim 10\%$. The fraction drops quickly toward other regions in the parameter space. The cyan dashed lines and asterisks highlight the fiducial QLF with $M^* = -25$, $\alpha = -1.3$, and $\beta = -2.7$, which has $F_{\rm multi} \sim 1\%$–2% for the brightest quasars and $F_{\rm multi} \sim 0.4\%$–0.8% for the depths of current surveys.

e.g., Barone-Nugent et al. 2015). Applying a single FJR without scatters will not accurately reproduce the VDF. Second, the FJRs are usually calibrated for massive galaxies with $\log \sigma \gtrsim 2.3$ (e.g., Focardi & Malavasi 2012), which might not describe less massive galaxies correctly.

(2) Directly adopt the VDF from galaxy surveys. Most previous studies of this kind adopted the local VDF in Choi et al. (2007) and assumed no redshift evolution. For example, Wyithe et al. (2011) calculated the lensing optical depth out to $z_s \sim 11$ and gave $\tau_m = 3 \times 10^{-3}$ for $z_s = 6$. Recent observations have suggested that the number density of massive galaxies decreases toward high redshifts (e.g., Chae 2010; Bezanson et al. 2012), indicating that a non-evolving VDF overestimates the lensing optical depth. As shown in Figure 1, at $z_d \gtrsim 0.9$, the Choi et al. (2007) VDF is higher than the observations and the VDFs in this study, which explains the difference in the predicted τ_m. Deflectors at this redshift range dominate the lensing optical depth (Figure 2). This comparison illustrates the importance of using a redshift-evolving VDF.

In addition to using VDFs to describe the deflector population, some studies also use cosmological simulations to calculate the lensing optical depth. For example, Hilbert et al. (2008) used the matter distribution from the Millennium simulation (Springel et al. 2005) and performed ray-tracing to model the strong-lensing statistics. They predict a lensing optical depth that is comparable to our results ($\tau_m \sim 1.2 \times 10^{-3}$ at $z_s = 5.7$).

To summarize, it is critical to have an accurate description of the deflector population when modeling the lensing statistics. The VDFs adopted by previous studies may have significant uncertainties (usually overestimated), which could bias the predicted lensing optical depth by a factor of ∼2–4. By applying recent measurements of VDFs, we reach a lower lensing optical depth and thus lower lensed fraction, which relieves the tension between the theoretical models and the observations. Since the VDFs at $z_d \gtrsim 1.5$ are still largely unconstrained, the predicted τ_m in our model also have some systematic errors. We estimate this uncertainty to be ∼30% by comparing the analytical VDF and the CosmoDC2 VDF, which are in good agreement at $z_d \lesssim 1.5$ but show more differences at higher redshifts. After taking the uncertainties into account, the difference between the observed lensed fraction ($F_{\rm multi} \approx 0.2\%$) and our model prediction ($F_{\rm multi} \approx 0.4\%$–$0.8\%$) is marginal.

We then consider the magnification bias B. Previous studies explored a wide range of QLF parameters, and the results are similar to this study. This is largely due to the fact that SIS

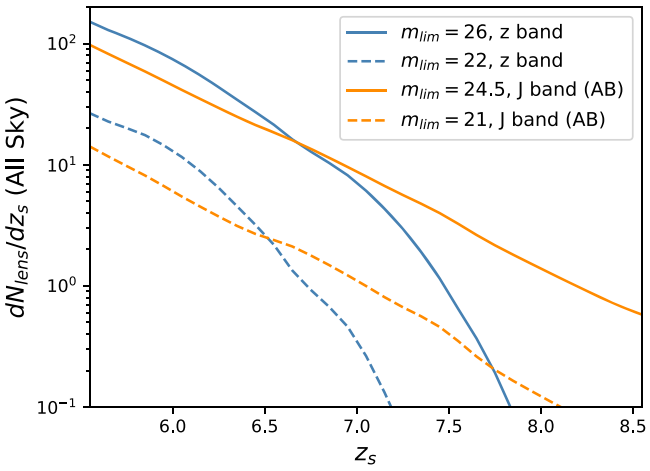

Figure 6. Numbers of detectable lensed quasars as a function of survey depth and quasar redshift. The solid lines correspond to the depths of the LSST survey ($m_z \approx 22$) and the Euclid survey ($m_{J,\rm AB} \approx 24.5$), and the dashed lines are depths of current imaging surveys (see text for details). Current sky surveys (optical + NIR) can detect ∼15 lensed quasars at $z_s > 5.5$ over the whole sky. The LSST survey can detect ∼45 lensed quasars at $z_s > 5.5$ in its footprint, and the Euclid survey can detect ∼4 at $z_s > 6.5$.

accurately describes the magnification distribution, $p(\mu)$, as suggested by Figure 4. However, it is worth noticing that most of the previous studies used the SDSS quasar survey depth ($m_{\rm lim} = 20.2$) when predicting the lensed fraction. Present-day high-redshift quasar surveys have depths of $m_{\rm lim} \gtrsim 22$, which lead to a lower expected lensed fraction than the SDSS depth.

5.2. The Number of Detectable High-redshift Lensed Quasars in Current and Future Sky Surveys

Large and deep imaging surveys (e.g., the LSST survey and the Euclid survey Scaramella et al. 2021) will greatly enhance our ability to find high-redshift quasars. In this section, we estimate the number of high-redshift lensed quasars that can be detected in current and future sky surveys.

We use the analytical model to calculate the number of lensed quasars that can be detected given a certain survey depth.[4] Specifically, we estimate the number of quasars that are intrinsically brighter than the survey limit using the QLF from Matsuoka et al. (2018), then calculate the number of detectable strongly lensed quasars using Equation (3). To convert apparent magnitudes to absolute magnitudes for quasars at redshift z_s, we generate mock quasars at $z_s - 0.1 < z_{\rm mock} < z_s + 0.1$ following the method in Section 3, and adopt the median value of $m - M_{1450}$ of these mock quasars. Since the majority of the $z_s \sim 6$ lenses will be resolved in upcoming sky surveys that have resolutions of $\lesssim 0\farcs7$, we use the magnification bias for the brightest image, $B = B_1$.

Figure 6 presents the predicted number density of lensed quasars that have the brightest lensed image detectable as a function of survey depth and redshift. We first consider optical imaging surveys, for which we use their z-band depths to compute the number of detectable lensed quasars. Current optical surveys have a typical depth of $m_z = 22$ (e.g., the DESI Legacy Imaging Survey, Dey et al. 2019), yielding 14 detectable lensed quasars at $z_s > 5.5$ over the whole sky. The LSST survey will reach a depth of $m_z \approx 26$, with which we can detect 89 lensed quasars at $z_s > 5.5$ over the whole sky (∼45 over the 20,000 deg^2 LSST footprint).

For quasars at $z_s \gtrsim 6.5$, the Lyα wavelength is redshifted to $\lambda_{\rm obs} \gtrsim 9120$ Å, and a substantial fraction of flux in z-band is absorbed by the highly neutral intergalactic medium. Consequently, the numbers of detectable lensed quasars in optical surveys drop quickly at this redshift range. We thus consider the expected outputs of near-infrared (NIR) imaging surveys. Present-day NIR surveys like the UKIRT Hemisphere Survey (Dye et al. 2018) and the VISTA Hemisphere Survey (McMahon et al. 2013) have depths of $m_J \approx 21$ (AB magnitude), leading to ∼1–2 detectable lensed quasars at $z_s > 6.5$ over the entire sky. In the upcoming Euclid survey that will reach a depth of $m_J = 24.5$, there will be 12 detectable lensed quasars at $z_s > 6.5$ over the sky (∼4 over the 14,000 deg^2 Euclid footprint).

To summarize, current sky surveys can only detect about 15 lensed quasars at $z_s > 5.5$ over the entire sky. Next-generation sky surveys are needed to build the first large sample of high-redshift lensed quasars. Besides, our model predicts that the Euclid survey can only detect ∼0.6 lensed quasars at $z_s > 7.5$, meaning that we are not likely to find a lensed quasar beyond this redshift in the near future.

Note that the numbers quoted above correspond to *detectable* lensed quasars; the outputs of real surveys heavily depend on the completeness of candidate selection methods and can be exceedingly complicated (see related discussion in Yue et al. 2021, submitted). If we only count the area with high galactic latitude (e.g., $|b| \gtrsim 30$ deg) and assume a high survey completeness (e.g., $\gtrsim$80%), the model suggests that we can only find a handful of lensed quasars at $z_s > 5.5$ in current sky surveys. The completeness of real surveys could be much lower (e.g., Fan et al. 2019; Pacucci & Loeb 2019). We expect that upcoming sky surveys like the LSST will find several tens of lensed quasars at $z_s > 5.5$.

6. Conclusion

We revisit the models of the high-redshift lensed quasar population, focusing on the lensed fraction $F_{\rm multi}$ of $z_s \sim 6$ quasars. We adopt recent measurements of VDFs and explore a wide range of QLF parameters, using both analytical methods and mock catalogs. Our models suggest a lensing optical depth of $\tau_m = 1.8 \times 10^{-3}$ for sources at $z_s = 6$, and a lensed fraction of $F_{\rm multi} \sim 0.4\%$–0.8% for ordinary QLF parameters and current survey depth ($m_{\rm lim} \approx 22$). For the brightest $z_s \sim 6$ quasars ($m_z \lesssim 19$), the fraction is ∼2% for ordinary QLF parameters and can be as high as ∼6% for steep QLF bright-end slopes.

By comparing our models to previous studies, we illustrate that it is critical to use an accurate, redshift-evolving VDF. Inaccurate VDFs will bias the predicted τ_m by a factor of several. Adopting VDFs from recent measurements relieves the tension between the observed lensed fraction and the model predictions. As the VDF at $z_d \gtrsim 2$ is still poorly constrained, we estimate that our model still has a systematic uncertainty of ∼30% for τ_m and thus $F_{\rm multi}$.

Finally, we estimate the number of high-redshift lensed quasars that can get detected in present-day and future imaging surveys. Our model suggests that there are ∼15 lensed quasars beyond the magnitude limit of current wide-area imaging surveys. Deeper surveys such as the LSST survey and the Euclid survey will find several tens of lensed quasars at $z_s > 5.5$

[4] The code for the analytical model is available at https://github.com/yuemh/lensQSOsim/tree/main/analytical.

and are necessary for building the first large sample of high-redshift lensed quasars.

We appreciate the valuable comments from Dr. Fabio Pacucci, Prof. Stuart Wyithe, and the anonymous referee. M. Y., X.F., and J.Y. acknowledge supports by NSF grants AST 19-08284. F.W. is thankful for the support provided by NASA through the NASA Hubble Fellowship grant #HST-HF2-51448.001-A awarded by the Space Telescope Science Institute, which is operated by the Association of Universities for Research in Astronomy, Incorporated, under NASA contract NAS5-26555.

ORCID iDs

Minghao Yue https://orcid.org/0000-0002-5367-8021
Xiaohui Fan https://orcid.org/0000-0003-3310-0131
Jinyi Yang https://orcid.org/0000-0001-5287-4242
Feige Wang https://orcid.org/0000-0002-7633-431X

References

Barone-Nugent, R. L., Wyithe, J. S. B., Trenti, M., et al. 2015, MNRAS, 450, 1224
Bezanson, R., van Dokkum, P., & Franx, M. 2012, ApJ, 760, 62
Chae, K.-H. 2010, MNRAS, 402, 2031
Choi, Y.-Y., Park, C., & Vogeley, M. S. 2007, ApJ, 658, 884
Comerford, J. M., Haiman, Z., & Schaye, J. 2002, ApJ, 580, 63
Dey, A., Schlegel, D. J., Lang, D., et al. 2019, AJ, 157, 168
Dye, S., Lawrence, A., Read, M. A., et al. 2018, MNRAS, 473, 5113
Faber, S. M., & Jackson, R. E. 1976, ApJ, 204, 668
Fan, X., Wang, F., Yang, J., et al. 2019, ApJL, 870, L11
Focardi, P., & Malavasi, N. 2012, ApJ, 756, 117
Geng, S., Cao, S., Liu, Y., et al. 2021, MNRAS, 503, 1319
Hasan, F., & Crocker, A. 2019, arXiv:1904.00486
Hilbert, S., White, S. D. M., Hartlap, J., & Schneider, P. 2008, MNRAS, 386, 1845
Jiang, L., McGreer, I. D., Fan, X., et al. 2016, ApJ, 833, 222
Ivezić, Ž., Kahn, S. M., Tyson, J. A., et al. 2019, ApJ, 873, 111
Kormann, R., Schneider, P., & Bartelmann, M. 1994, A&A, 284, 285
Korytov, D., Hearin, A., Kovacs, E., et al. 2019, ApJS, 245, 26
Kulkarni, G., Worseck, G., & Hennawi, J. F. 2019, MNRAS, 488, 1035
Mason, C. A., Treu, T., Schmidt, K. B., et al. 2015, ApJ, 805, 79
Matsuoka, Y., Strauss, M. A., Kashikawa, N., et al. 2018, ApJ, 869, 150
McGreer, I. D., Fan, X., Jiang, L., & Cai, Z. 2018, AJ, 155, 131
McGreer, I. D., Hall, P. B., Fan, X., et al. 2010, AJ, 140, 370
McGreer, I. D., Jiang, L., Fan, X., et al. 2013, ApJ, 768, 105
McMahon, R. G., Banerji, M., Gonzalez, E., et al. 2013, Msngr, 154, 35
More, A., Oguri, M., Kayo, I., et al. 2016, MNRAS, 456, 1595
Oguri, M. 2010, glafic: Software Package for Analyzing Gravitational Lensing, Astrophysics Source Code Library, ascl:1010.012
Oguri, M., & Marshall, P. J. 2010, MNRAS, 405, 2579
Pacucci, F., & Loeb, A. 2019, ApJL, 870, L12
Pei, Y. C. 1995, ApJ, 438, 623
Richards, G. T., Fan, X., Newberg, H. J., et al. 2002, AJ, 123, 2945
Richards, G. T., Haiman, Z., Pindor, B., et al. 2006, AJ, 131, 49
Richards, G. T., Strauss, M. A., Pindor, B., et al. 2004, AJ, 127, 1305
Scaramella, R., Amiaux, J., Mellier, Y., et al. 2021, arXiv:2108.01201
Schneider, P., Ehlers, J., & Falco, E. E. 1992, Gravitational Lenses (Berlin: Springer)
Sohn, J., Zahid, H. J., & Geller, M. J. 2017, ApJ, 845, 73
Springel, V., White, S. D. M., Jenkins, A., et al. 2005, Natur, 435, 629
Wang, F., Yang, J., Fan, X., et al. 2019, ApJ, 884, 30
Wang, F., Yang, J., Fan, X., et al. 2021, ApJL, 907, L1
Wyithe, J. S. B., & Loeb, A. 2002, ApJ, 577, 57
Wyithe, J. S. B., Yan, H., Windhorst, R. A., & Mao, S. 2011, Natur, 469, 181
Yang, J., Venemans, B., Wang, F., et al. 2019a, ApJ, 880, 153
Yang, J., Wang, F., Fan, X., et al. 2019b, ApJ, 871, 199
Yang, J., Wang, F., Fan, X., et al. 2020, ApJL, 897, L14
York, D. G., Adelman, J., Adelman, J. E. J., et al. 2000, AJ, 120, 1579
Yue, M., Yang, J., Fan, X., et al. 2021, ApJ, 917, 99